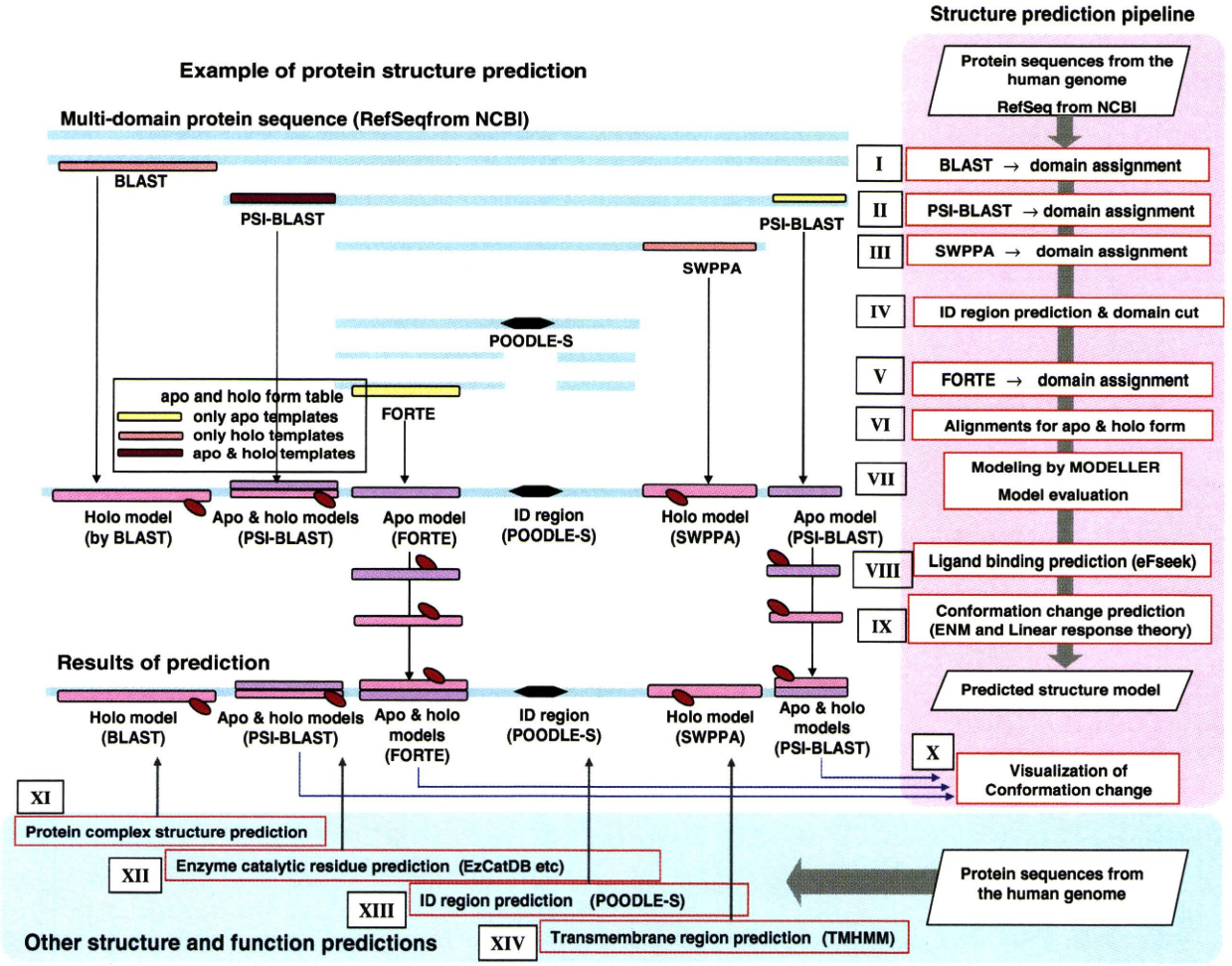

Figure 1. SAHG prediction systems. 'Structure prediction pipeline' and 'Other structure and function predictions' are shown in the right pink regions and bottom light-blue regions, respectively. The center panel illustrates each procedure in the flow of the structure prediction pipeline, showing how the results of systems are integrated. SWPPA: Smith–Waterman profile–profile alignment method; ID: intrinsically disordered; ENM: elastic network model.

and holo form table' originally prepared by us (see 'Apo and holo form table' section in Supplementary data). For the template in apo form, the corresponding template (>90% sequence identity) in holo form was selected from the table and *vice versa*. For both the templates, alignments to target sequences were prepared (VI in Figure 1). In the model building and quality assessment step, 10 models were constructed using the MODELLER (30) software. The quality of the models was evaluated using Stability score (31) and the best 3D model for each alignment was chosen (VII in Figure 1).

As of July 2010, 24 878 RefSeq sequences [(22), 14 012 591 residues] encoded in the human genome were processed by the pipeline. In total, 42 581 structure models were constructed, of which 18 228, 14 577, 9163 and 613 templates were detected by BLAST, PSI-BLAST, SWPPA and FORTE, respectively. For 4083 models (9% of all models), both the apo and holo forms were assigned. In total, 35 275 residues were predicted to form long ID regions and removed from target sequences, in advance of the FORTE search. In total, 295 309 residues were eliminated because they were fragmented into small pieces (<26 residues). Multiple models were generated for 9057 RefSeq sequences, while only one model was generated for 12 310 RefSeq sequences. In total, 3511 RefSeq sequences remain without any predicted model. Note that one model does not necessarily correspond to one domain (sometimes it corresponds to a protein chain), but at least more than one-third of human proteins were estimated to be multi-domain proteins. In some cases, we assessed predictions by comparing models with the protein structures recently revealed. Even the sequence identities of the alignments are quite low (<20%), more than half predictions detect correct folds (Supplementary Table S1), indicating that our prediction pipeline worked well.

Treatments of multi domain proteins. Many human proteins are composed of multiple domains and contain a significant fraction of ID regions, as was described above. These factors often prevent predicting protein

structures in their full-length forms. As a result, SAHG principally exhibits protein structure as an array of domains. However, when multi-domain structures are available in the templates, the prediction pipeline implicitly prioritizes them to take advantage of the relative domain orientations. The pool of templates consists of SCOP (24,25) domains and whole PDB (7) structures, some of which are not deposited in SCOP. At the template assignment step (I, II, III, V in Figure 1), a set of templates was chosen to maximize the length of modeled regions. This approach is effective in accepting PDB structures spanning multiple domains, as the templates.

Prediction of potential domains. ID regions were predicted using the POODLE-S (18) software, which calculates the probability of being in ID regions for each residue (XIII in Figure 1). As ID regions are considered to play fundamental roles in biological activities (17), their detections should be important. On the other hand, it is necessary to remove long ID regions from the target sequences and assign potential domain regions to assure better performance in structure prediction (FORTE search, V in Figure 1). For this purpose, we evaluated an existing method to predict domain boundaries [Domcut (32)] and found that it was likely to overcut potential domain regions into segments. For other methods (33–35), the same tendency was reported. We considered that the over-prediction was rather disadvantageous for arranging the input sequences for FORTE and developed a new method whose prediction was more 'moderate' (containing fewer false positives but more false negatives) based on the results of ID region prediction (IV in Figure 1), since ID regions act as linkers of structural domains (36). First, the results of POODLE-S for a target sequence were converted into a binary sequence in which 0 ($P < 0.5$) and 1 represent residues in structured regions and that in ID regions, respectively. Next, to detect regions where 0 were continuously abundant, we employed a simple two-state Hidden Markov Model. In this model, one state, 'a mostly structured region' (STR), emits 0 more frequently than 1 and the other state, 'a mostly ID region' (IDR), emits 1 more frequently than 0. The transition probability between STR and IDR and all the emission probabilities were empirically adjusted to eliminate over-prediction by referring to known domain data in PDB. Finally, the STR regions were estimated from the input binary sequence by calculating a Viterbi path.

Prediction of conformational change upon ligand binding. When templates for both the ligand-bound state (holo form) and unbound state (apo form) were detected using the 'apo and holo form table', two types of models were constructed and their structural changes upon ligand-binding are visualized by means of a morphing technique (the MORPH2 program in Martz-Authored PDB Tools see http://www.umass.edu/microbio/rasmol/pdbtools.htm) (X in Figure 1). The animation of conformational change provides significant information for protein function when it is shown with functional residues and ligands.

When there was only the template for apo form available and accordingly, only the model for apo form was constructed, its putative ligand and the binding sites were predicted by the eF-seek software (37) (VIII in Figure 1). eF-seek finds potential ligand-binding sites in the model of the apo form, if similar structures were deposited in eF-site, the database of representative ligand-binding sites (38). eF-seek employs a clique search algorithm. As this method is sensitive to the input 3D coordinates, the application was limited to the case of highly accurate structure models being available, i.e. the templates were detected by BLAST search with more than 90% sequence identity to the target sequences. The structural changes upon the predicted ligand-binding were then deduced using the elastic network model (39) and linear response theory to construct a model of the holo form (40) (IX in Figure 1).

Note that this approach and presentation is one of the key features of the SAHG database. Animated views of the conformational change of the domains upon ligand-binding could present a deep insight into the protein structure and function relationship (X in Figure 1). As of July 2010, conformational changes upon ligand-binding were predicted for 4083 modeled domains among 42 581 3D models.

Other structure and function predictors

Prediction of protein complex structure. In total, 33 687 protein complex structures were gathered from the PQS database (41). If all the subunits from two complexes were paired with more than 95% sequence identity, the complexes were clustered together in the single-linkage manner. The complex structure with the highest resolution was selected in each cluster of complexes and we obtained a non-redundant set composed of 12 730 template complexes. If a target sequence was related to a given subunit of a template complex with >80% sequence identity by the BLAST search and all the other subunits were related to any target sequences, the complex model was constructed by MODELLER. In total, 8667 complex models were prepared for 3650 target sequences (XI in Figure 1).

Ligand binding information. The ligands and their binding sites were retrieved from constructed models. The ligands were mainly small molecules, such as peptides, nucleotides, metal ions, etc. and some trivial chemicals from buffers or precipitants were excluded. Binding sites were residues whose distances from any ligand atoms were within 5 Å.

Prediction of catalytic residues. For the target sequences of enzymes, catalytic residues were predicted using the EzCatDB database (42) (XII in Figure 1). The EzCatDB database provides annotations on catalytic residues with PDB structure data. The catalytic residues and their positions were already denoted for sequences in the UniProt database (6), as mapped from the catalytic residues on the PDB sequence data, by BLAST search with 10^{-10} *E*-value cut-off and POA ver. 2.0 (43). From the human proteins in the UniProt database, target sequences were detected and catalytic residues were assigned in the same manner. Only

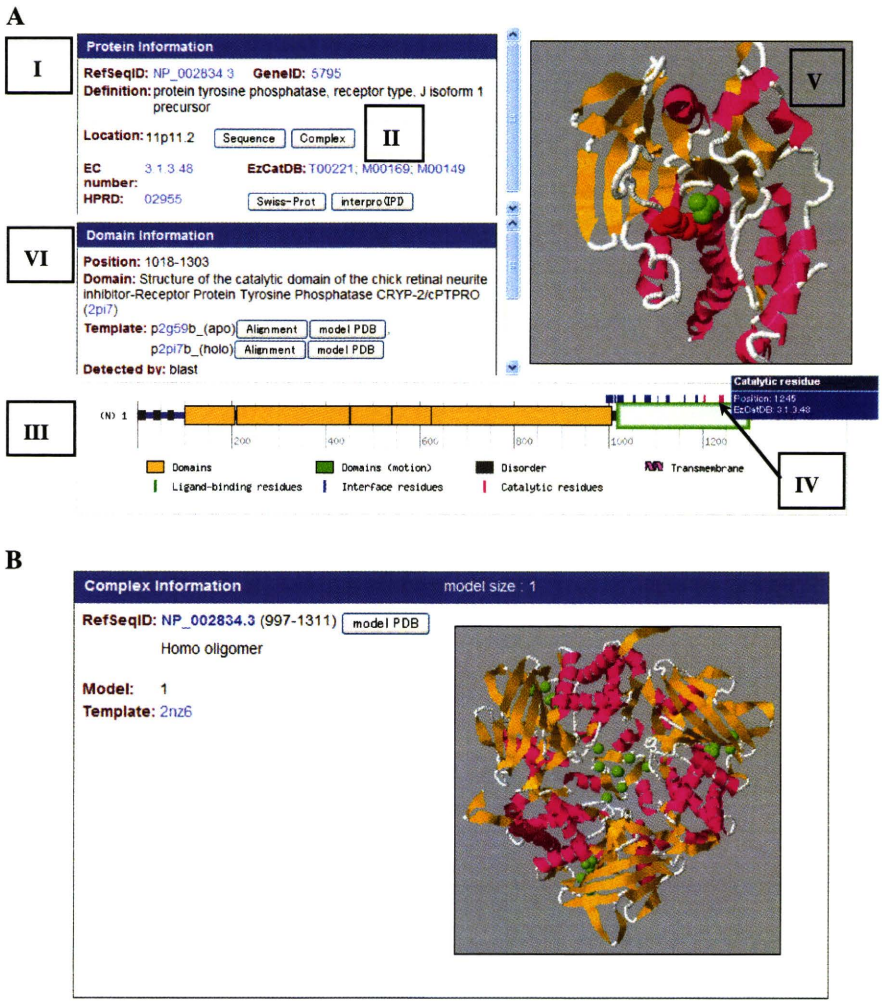

Figure 2. (**A**) Example view of SAHGs detailed information page [RefSeqID: NP_002834.3, protein tyrosine phosphatase, receptor type, J isoform 1 precursor (48)]. Labels I, II, III, IV, V and VI indicate the 'Protein information' panel, the 'Complex' button, the 'bar indicator', the 'Domain information' panel, the 'Jmol Window' and the 'Catalytic residue' pin on the bar indicator, respectively. (**B**) Example view of a 'Complex information' page (NP_002834.3). For this protein, only one complex structure in a homo-trimeric form was predicted.

chemically consistent residues were regarded as catalytic residues. The annotated 'ACT_SITE' residues for the human proteins in the UniProt database were also mapped on the target sequences using BLAST search.

Prediction of ID and transmembrane regions. ID regions were predicted by the POODLE-S software (XIII in Figure 1). Transmembrane regions were assigned by the TMHMM software (44) (XIV in Figure 1). If these predicted regions were overlapped with 3D models, the latter take priority over the former.

ACCESS AND INTERFACE

SAHG provides its graphical web interface at http://bird.cbrc.jp/sahg. By clicking a chromosome's image, all proteins coded in the chromosome are listed with the predicted models. By choosing an image of a domain, detailed information of the target protein is shown. More practically, detailed information of specific proteins can be accessed by querying with Gene ID, RefSeq ID, annotation keywords or their combinations or by sequence homology search (BLAST), from an 'Advanced search page'. In the detailed information page (Figure 2A), all contents for a given protein are shown. The 'Protein information' panel provides the information of the protein's RefSeq ID (I in Figure 2A). The sequence in FASTA format is displayed by clicking a 'Sequence' button. Predicted protein complexes are shown via a 'Complex' button if available (II in Figure 2A). An example of a 'complex information' page is shown in Figure 2B. Links to EC number, EzCatDB (42), HPRD (45), Swiss-Prot(6) and InterPro (46) are provided if available. A bar indicator is convenient for seeing the position of the predicted models in the full-length protein (III in Figure 2A). It also shows the annotation of ligand-binding

residues (retrieved from the holo models), protein–protein interface residues (from protein complexes), catalytic residues (from EzCatDB), ID regions (by POODLE-S) and transmembrane regions (by TMHMM). By pointing at the colored pins on the bar indicator with a mouse, precise locations (residue numbers) of ligand-binding residues (green pins), protein–protein interface residues (blue) or catalytic residues (red) are shown (see IV in Figure 2A, an example of a catalytic residue). When a modeled region in the bar indicator (blocks on the bar) is selected by clicking, the predicted 3D model appears in the Jmol window (an open-source Java viewer for chemical structures in 3D; see http://www.jmol.org/Jmol) (V in Figure 2A). When models of both apo and holo forms are available (green block on the bar), their structural changes upon ligand-binding are visualized by the morphing technique (the MORPH2 program in Martz-Authored PDB Tools; see http://www.umass.edu/microbio/rasmol/pdbtools.htm) and displayed as an animated image including the ligand molecules in this window. By clicking the bar indicator of ligand-binding or catalytic residues, the corresponding residues are highlighted in 'CPK spacefill' scheme in the Jmol window. The 'Domain Information' panel shows structural and functional information about a selected model (VI in Figure 2A). The target sequence-template alignments are displayed by an 'Alignment button'. The predicted model can be downloaded in a pdb format via 'model PDB' button. Ligand-binding residues, protein–protein interface residues and catalytic residues are also listed as 'Functional Residues' in the same color of the bar indicator. (In Figure 2A, the 'Domain information' panel should be scrolled up).

FUTURE DIRECTIONS

To improve the accuracy of structure prediction we are implementing a probabilistic profile–profile alignment method in our prediction pipeline. The method is an enhanced version of the probabilistic sequence–sequence alignment method (47), which has been proven to perform better than PSI-BLAST, in particular for orphan proteins. New versions of structure models provided by the new pipeline will appear in fall of 2010. The results of predictions are being examined to clarify the function and the interaction of human proteins. For some proteins, predicted ligands are being verified experimentally. The structure model set in SAHG will be downloadable in bulk in future.

SUPPLEMENTARY DATA

Supplementary Data are available at NAR Online.

ACKNOWLEDGEMENTS

The authors are grateful to Takatsugu Hirokawa and Kiyoshi Asai for their support of the project, to Martin Frith for his critical reading of the article and to Mari Saito for her contribution to website design.

FUNDING

Japan Science and Technology Agency (JST) – Institute for Bioinformatics Research and Development (BIRD). Funding for open access charge: National Institute of Advanced Industrial Science and Technology (AIST).

Conflict of interest statement. None declared.

REFERENCES

1. Nelson,K.E., Weinstock,G.M., Highlander,S.K., Worley,K.C., Creasy,H.H., Wortman,J.R., Rusch,D.B., Mitreva,M., Sodergren,E., Chinwalla,A.T. *et al.* (2010) A catalog of reference genomes from the human microbiome. *Science*, **328**, 994–999.
2. Drmanac,R., Sparks,A.B., Callow,M.J., Halpern,A.L., Burns,N.L., Kermani,B.G., Carnevali,P., Nazarenko,I., Nilsen,G.B., Yeung,G. *et al.* (2010) Human genome sequencing using unchained base reads on self-assembling DNA nanoarrays. *Science*, **327**, 78–81.
3. Zhang,W. and Dolan,M.E. (2010) Impact of the 1000 genomes project on the next wave of pharmacogenomic discovery. *Pharmacogenomics*, **11**, 249–256.
4. Metzker,M.L. (2010) Sequencing technologies - the next generation. *Nat. Rev. Genet.*, **11**, 31–46.
5. MacLean,D., Jones,J.D. and Studholme,D.J. (2009) Application of 'next-generation' sequencing technologies to microbial genetics. *Nat. Rev. Microbiol.*, **7**, 287–296.
6. Consortium,U. (2010) The Universal Protein Resource (UniProt) in 2010. *Nucleic Acids Res.*, **38**, D142–D148.
7. Deshpande,N., Addess,K.J., Bluhm,W.F., Merino-Ott,J.C., Townsend-Merino,W., Zhang,Q., Knezevich,C., Xie,L., Chen,L., Feng,Z. *et al.* (2005) The RCSB Protein Data Bank: a redesigned query system and relational database based on the mmCIF schema. *Nucleic Acids Res.*, **33**, D233–D237.
8. Xie,L. and Bourne,P.E. (2005) Functional coverage of the human genome by existing structures, structural genomics targets, and homology models. *PLoS Comput. Biol.*, **1**, e31.
9. Thornton,J.M., Todd,A.E., Milburn,D., Borkakoti,N. and Orengo,C.A. (2000) From structure to function: approaches and limitations. *Nat. Struct. Biol.*, **7(Suppl.)**, 991–994.
10. Cozzetto,D., Kryshtafovych,A., Fidelis,K., Moult,J., Rost,B. and Tramontano,A. (2009) Evaluation of template-based models in CASP8 with standard measures. *Proteins*, **77(Suppl. 9)**, 18–28.
11. Kopp,J., Bordoli,L., Battey,J.N., Kiefer,F. and Schwede,T. (2007) Assessment of CASP7 predictions for template-based modeling targets. *Proteins*, **69(Suppl. 8)**, 38–56.
12. Grant,M.A. (2009) Protein structure prediction in structure-based ligand design and virtual screening. *Comb. Chem. High Throughput Screen*, **12**, 940–960.
13. Katritch,V., Rueda,M., Lam,P.C., Yeager,M. and Abagyan,R. (2010) GPCR 3D homology models for ligand screening: lessons learned from blind predictions of adenosine A2a receptor complex. *Proteins*, **78**, 197–211.
14. Zhang,Y. (2009) I-TASSER: fully automated protein structure prediction in CASP8. *Proteins*, **77(Suppl. 9)**, 100–113.
15. Apic,G., Gough,J. and Teichmann,S.A. (2001) Domain combinations in archaeal, eubacterial and eukaryotic proteomes. *J. Mol. Biol.*, **310**, 311–325.
16. Dunker,A.K., Obradovic,Z., Romero,P., Garner,E.C. and Brown,C.J. (2000) Intrinsic protein disorder in complete genomes. *Genome Inform. Ser. Workshop Genome Inform.*, **11**, 161–171.
17. Dunker,A.K., Silman,I., Uversky,V.N. and Sussman,J.L. (2008) Function and structure of inherently disordered proteins. *Curr. Opin. Struct. Biol.*, **18**, 756–764.
18. Shimizu,K., Muraoka,Y., Hirose,S., Tomii,K. and Noguchi,T. (2007) Predicting mostly disordered proteins by using structure-unknown protein data. *BMC Bioinformatics*, **8**, 78.
19. Ward,J.J., Sodhi,J.S., McGuffin,L.J., Buxton,B.F. and Jones,D.T. (2004) Prediction and functional analysis of native disorder in proteins from the three kingdoms of life. *J. Mol. Biol.*, **337**, 635–645.

20. Kiefer,F., Arnold,K., Kunzli,M., Bordoli,L. and Schwede,T. (2009) The SWISS-MODEL Repository and associated resources. *Nucleic Acids Res.*, **37**, D387–D392.
21. Pieper,U., Eswar,N., Webb,B.M., Eramian,D., Kelly,L., Barkan,D.T., Carter,H., Mankoo,P., Karchin,R., Marti-Renom,M.A. *et al.* (2009) MODBASE, a database of annotated comparative protein structure models and associated resources. *Nucleic Acids Res.*, **37**, D347–D354.
22. Pruitt,K.D., Tatusova,T., Klimke,W. and Maglott,D.R. (2009) NCBI Reference Sequences: current status, policy and new initiatives. *Nucleic Acids Res.*, **37**, D32–D36.
23. Altschul,S.F., Madden,T.L., Schaffer,A.A., Zhang,J., Zhang,Z., Miller,W. and Lipman,D.J. (1997) Gapped BLAST and PSI-BLAST: a new generation of protein database search programs. *Nucleic Acids Res.*, **25**, 3389–3402.
24. Andreeva,A., Howorth,D., Chandonia,J.M., Brenner,S.E., Hubbard,T.J., Chothia,C. and Murzin,A.G. (2008) Data growth and its impact on the SCOP database: new developments. *Nucleic Acids Res.*, **36**, D419–D425.
25. Chandonia,J.M., Hon,G., Walker,N.S., Lo Conte,L., Koehl,P., Levitt,M. and Brenner,S.E. (2004) The ASTRAL Compendium in 2004. *Nucleic Acids Res.*, **32**, D189–D192.
26. Wang,G. and Dunbrack,R.L. Jr (2004) Scoring profile-to-profile sequence alignments. *Protein Sci.*, **13**, 1612–1626.
27. Tomii,K. and Akiyama,Y. (2004) FORTE: a profile-profile comparison tool for protein fold recognition. *Bioinformatics*, **20**, 594–595.
28. Tomii,K., Hirokawa,T. and Motono,C. (2005) Protein structure prediction using a variety of profile libraries and 3D verification. *Proteins*, **61(Suppl. 7)**, 114–121.
29. Thornton,J.M., Orengo,C.A., Todd,A.E. and Pearl,F.M. (1999) Protein folds, functions and evolution. *J. Mol. Biol.*, **293**, 333–342.
30. Sali,A. and Blundell,T.L. (1993) Comparative protein modelling by satisfaction of spatial restraints. *J. Mol. Biol.*, **234**, 779–815.
31. Ota,M., Isogai,Y. and Nishikawa,K. (2001) Knowledge-based potential defined for a rotamer library to design protein sequences. *Protein Eng.*, **14**, 557–564.
32. Suyama,M. and Ohara,O. (2003) DomCut: prediction of inter-domain linker regions in amino acid sequences. *Bioinformatics*, **19**, 673–674.
33. Cheng,J. (2007) DOMAC: an accurate, hybrid protein domain prediction server. *Nucleic Acids Res.*, **35**, W354–W356.
34. Ebina,T., Toh,H. and Kuroda,Y. (2009) Loop-length-dependent SVM prediction of domain linkers for high-throughput structural proteomics. *Biopolymers*, **92**, 1–8.
35. Kim,D.E., Chivian,D., Malmstrom,L. and Baker,D. (2005) Automated prediction of domain boundaries in CASP6 targets using Ginzu and RosettaDOM. *Proteins*, **61(Suppl. 7)**, 193–200.
36. Dyson,H.J. and Wright,P.E. (2005) Intrinsically unstructured proteins and their functions. *Nat. Rev. Mol. Cell Biol.*, **6**, 197–208.
37. Kinoshita,K., Murakami,Y. and Nakamura,H. (2007) eF-seek: prediction of the functional sites of proteins by searching for similar electrostatic potential and molecular surface shape. *Nucleic Acids Res.*, **35**, W398–W402.
38. Kinoshita,K. and Nakamura,H. (2004) eF-site and PDBjViewer: database and viewer for protein functional sites. *Bioinformatics*, **20**, 1329–1330.
39. Tirion,M.M. (1996) Large Amplitude Elastic Motions in Proteins from a Single-Parameter, Atomic Analysis. *Phys. Rev. Lett.*, **77**, 1905–1908.
40. Ikeguchi,M., Ueno,J., Sato,M. and Kidera,A. (2005) Protein structural change upon ligand binding: linear response theory. *Phys. Rev. Lett.*, **94**, 078102.
41. Henrick,K. and Thornton,J.M. (1998) PQS: a protein quaternary structure file server. *Trends Biochem. Sci.*, **23**, 358–361.
42. Nagano,N. (2005) EzCatDB: the enzyme catalytic-mechanism database. *Nucleic Acids Res.*, **33**, D407–D412.
43. Grasso,C. and Lee,C. (2004) Combining partial order alignment and progressive multiple sequence alignment increases alignment speed and scalability to very large alignment problems. *Bioinformatics*, **20**, 1546–1556.
44. Krogh,A., Larsson,B., von Heijne,G. and Sonnhammer,E.L. (2001) Predicting transmembrane protein topology with a hidden Markov model: application to complete genomes. *J. Mol. Biol.*, **305**, 567–580.
45. Keshava Prasad,T.S., Goel,R., Kandasamy,K., Keerthikumar,S., Kumar,S., Mathivanan,S., Telikicherla,D., Raju,R., Shafreen,B., Venugopal,A. *et al.* (2009) Human protein reference database–2009 update. *Nucleic Acids Res.*, **37**, D767–D772.
46. Hunter,S., Apweiler,R., Attwood,T.K., Bairoch,A., Bateman,A., Binns,D., Bork,P., Das,U., Daugherty,L., Duquenne,L. *et al.* (2009) InterPro: the integrative protein signature database. *Nucleic Acids Res.*, **37**, D211–D215.
47. Koike,R., Kinoshita,K. and Kidera,A. (2007) Probabilistic alignment detects remote homology in a pair of protein sequences without homologous sequence information. *Proteins*, **66**, 655–663.
48. Ostman,A., Yang,Q. and Tonks,N.K. (1994) Expression of DEP-1, a receptor-like protein-tyrosine-phosphatase, is enhanced with increasing cell density. *Proc. Natl Acad. Sci. USA*, **91**, 9680–9684.

THE JOURNAL OF BIOLOGICAL CHEMISTRY VOL. 285, NO. 22, pp. 16822–16829, May 28, 2010

A Common Substrate Recognition Mode Conserved between Katanin p60 and VPS4 Governs Microtubule Severing and Membrane Skeleton Reorganization*[S]

Received for publication, January 28, 2010 Published, JBC Papers in Press, March 25, 2010, DOI 10.1074/jbc.M110.108365

Naoko Iwaya[‡§¶], Yohta Kuwahara[§¶‖], Yoshie Fujiwara[§], Natsuko Goda[§‖], Takeshi Tenno[§‖], Kohei Akiyama[¶], Shogo Mase[§‖], Hidehito Tochio[‡], Takahisa Ikegami[‡‡], Masahiro Shirakawa[‡], and Hidekazu Hiroaki[§¶‖**1]**

*From the [‡]Department of Molecular Engineering, Graduate School of Engineering, Kyoto University, Kyoto-Daigaku Katsura, Nishikyo-ku, Kyoto 615-8530, the [§]Department of Biochemistry and Molecular Biology, Graduate School of Medicine, Kobe University, 7-5-1 Kusunokicho, Chuo-ku, Kobe, Hyogo 650-0017, the [¶]Field of Supramolecular Biology, International Graduate School of Arts and Sciences, Yokohama City University, Yokohama, Kanagawa 230-0045, the [‖]Institute for Bioinformatics Research and Development, Japan Science and Technology Corporation, Tokyo 102-0081, the **Global Center of Excellence Program for Integrative Membrane Biology, Kobe University, Kobe, Hyogo 650-0017, and the [‡‡]Institute of Protein Research, Osaka University, Suita, Osaka 565-0871, Japan*

Katanin p60 (kp60), a microtubule-severing enzyme, plays a key role in cytoskeletal reorganization during various cellular events in an ATP-dependent manner. We show that a single domain isolated from the N terminus of mouse katanin p60 (kp60-NTD) binds to tubulin. The solution structure of kp60-NTD was determined by NMR. Although their sequence similarities were as low as 20%, the structure of kp60-NTD revealed a striking similarity to those of the microtubule interacting and trafficking (MIT) domains, which adopt anti-parallel three-stranded helix bundle. In particular, the arrangement of helices 2 and 3 is well conserved between kp60-NTD and the MIT domain from Vps4, which is a homologous protein that promotes disassembly of the endosomal sorting complexes required for transport III membrane skeleton complex. Mutation studies revealed that the positively charged surface formed by helices 2 and 3 binds tubulin. This binding mode resembles the interaction between the MIT domain of Vps4 and Vps2/CHMP1a, a component of endosomal sorting complexes required for transport III. Our results show that both the molecular architecture and the binding modes are conserved between two AAA-ATPases, kp60 and Vps4. A common mechanism is evolutionarily conserved between two distinct cellular events, one that drives microtubule severing and the other involving membrane skeletal reorganization.

Microtubules (MTs)[2] are polymers of α- and β-tubulin heterodimers. MTs exist as networks that dynamically and rapidly reorganize during different phases of the cell cycle. Spontaneous growth as well as shortening at the ends is indispensable for functional rearrangement. For example, they form the mitotic spindle during M phase, which mediates chromosome segregation during cell division based on the nature of dynamic rearrangement of MTs (reviewed in Refs. 1, 2). Many cellular events involving MTs are driven not only by autonomous polymerization and dissociation of tubulin but also by MT-severing enzymes. These enzymes disassemble the MTs to promote large changes in the cytoskeleton in an ATP-dependent manner (3).

There are three known MT-severing enzymes, katanin, spastin, and fidgetin, all of which belong to type I AAA-ATPases (4–7). Katanin was first identified from sea urchin cytosol (8) and consists of two subunits as follows: a 60-kDa catalytic subunit (kp60) containing a single AAA domain, and an 80-kDa regulatory subunit (kp80) (9, 10). Both the subunits are genetically conserved among many higher eukaryotes. Katanin localizes at the centrosomes in an MT-dependent manner (11), which is probably required for recycling and for the poleward flux of tubulin in the spindle by disassembling MTs at their minus ends (12, 13). kp60 homologs are also found in plants, insects, and nematodes but not in yeasts.

kp60 has a common domain organization typical of a type I AAA-ATPase, which consists of an N-terminal substrate binding region followed by a single AAA domain at the C terminus. In general, AAA-ATPases are believed to act as protein unfoldases that promote various cellular events, including dissociation of protein complexes, MT severing, protein degradation, protein translocation across organelle membranes, vesicle fusions, and multivesicular body formation (reviewed in Refs. 14, 15).

Hartman and Vale (13) demonstrated that the N-terminal half of kp60 contains an MT binding region, although the presence of a structural MT binding domain was not proved. The importance of the N-terminal MT binding region of a plant kp60 ortholog has been recently reported (16). In our previous study, we successfully isolated a folded structural domain from the kp60 N-terminal region (termed kp60-NTD) (17). Al-

* A part of this work was performed under the Cooperative Research Program of Institute for Protein Research, Osaka University.

[S] The on-line version of this article (available at http://www.jbc.org) contains supplemental "Experimental Procedures," Figs. 1–8, Table 1, and additional references.

[1] To whom correspondence should be addressed. Tel.: 81-78-382-5813; Fax: 81-78-382-5816; E-mail: hiroakih@med.kobe-u.ac.jp.

[2] The abbreviations used are: MT, microtubule; AAA, ATPase associated with various cellular activities; ESCRT, endosomal sorting complexes required for transport; GST, glutathione *S*-transferase; kp60, katanin p60; MIT domain, microtubule interacting and trafficking domain; r.m.s.d., root mean square deviation; NTD, N-terminal domain; PIPES, 1,4-piperazinediethanesulfonic acid; PDB, Protein Data Bank.

though standard bioinformatics tools (*e.g.* PSI-BLAST (18), Pfam (19, 20), and SMART (21)) failed to detect any similarity between kp60-NTD and other known domains, more sensitive bioinformatics techniques (*e.g.* FORTE (22) and FUGUE (23)) can detect substantial similarities between kp60-NTD and MIT domains. MIT domains are small helical domains involved in protein-protein interactions that are conserved among Vps4, spartin, spastin, and some other proteins (24).

In this study, we present the solution structure of kp60-NTD. We show that this structure is closely related to that of the MIT domain. In this context, the overall molecular architecture of kp60 resembles other MIT domain-containing type I AAA-ATPases, such as the MT-severing enzyme spastin and the ESCRT-III disassembling enzyme Vps4 (Fig. 1*A*). Because the isolated kp60-NTD solely binds tubulin *in vitro*, the domain is a novel tubulin binding domain. Finally, the key residues of kp60-NTD for binding tubulin were determined. A model for MT binding is further discussed, which allows us to propose a model for the mechanism of MT severing by katanin.

EXPERIMENTAL PROCEDURES

Protein Techniques—Expression vectors for the recombinant GST-tagged form of kp60-NTDs of human and mouse were constructed using PRESAT vector methodology (17, 25). The fusion proteins were expressed in *Escherichia coli* BL21 (DE3), followed by affinity purification on glutathione-Sepharose (GE Healthcare), and were dialyzed. These fusion proteins were used for tubulin binding assays. For NMR spectroscopy, 2 liters of culture was incubated with [^{15}N]ammonium chloride and [^{13}C]glucose as the sole nitrogen and carbon sources, respectively, following a standard fermentation protocol at 25 °C. Divalent cation was present as a trace mineral during fermentation. Purification of ^{15}N- and ^{13}C-/^{15}N-labeled kp60-NTDs was achieved by glutathione-Sepharose affinity chromatography followed by thrombin digestion, benzamidine-Sepharose chromatography, cation exchange chromatography using a SP-Sepharose column, and gel filtration using Superdex 75 column (GE Healthcare).

NMR Spectroscopy—Samples for NMR spectroscopy contained either ^{15}N- or ^{13}C-/^{15}N-labeled kp60-NTD at concentrations of 0.5–0.9 mM in 5% D_2O, 95% H_2O, 20 mM sodium phosphate, and 1 mM EDTA with 50 mM NaCl/without NaCl (pH 6.5). Backbone and side chain assignments were obtained from ^{15}N-heteronuclear single quantum coherence spectroscopy, ^{13}C-heteronuclear single quantum coherence spectroscopy, HNCA, HNCO, HNCACB, CBCACONH, HCC(CO)NH, CC(CO)NH, and HCCH-total correlation spectroscopy spectra recorded at 25 °C, using Bruker Avance spectrometers (500 and 800 MHz, Avance; Bruker Biospin, Germany) equipped with cryomagnetic probes (26, 27). Data were processed using NMRPipe (28) and SPARKY (29) software. Interproton distances were obtained from three-dimensional ^{13}C- and ^{15}N-edited nuclear Overhauser effect spectroscopy spectra recorded with a 100-ms mixing time. Structures were calculated using a standard seven iteration cycle protocol of the program CYANA version 2.0.17 (30, 31). All nuclear Overhauser effect cross-peaks were selected manually using SPARKY. In total, 1723 meaningful nuclear Overhauser effect upper distance restraints were obtained, including 304 long range distances. Dihedral angle restraints were calculated on the basis of backbone atom chemical shifts (32) using the TALOS program. The 20 structures with the lowest restraint energies were selected and analyzed using MOLMOL (33) and PROCHECK-NMR software (Table 1) (34). No distance restraint was violated by more than 0.3 Å and no torsional restraint by more than 5.0°. All the figures were prepared using MOLMOL and PyMOL. The atomic coordinates of the 20 best kp60-NTD NMR structures have been deposited in the Protein Data Bank under accession code 2rpa. Chemical shift assignments have been deposited in the BioMagResBank under accession code 11075.

Mutation Studies and Tubulin Binding Assays—Ala-substituted mutants were prepared by PCR amplification of the entire expression plasmid for kp60-NTD (residues 1–72) according to a standard PCR mutagenesis method using QuikChange site-directed mutagenesis kit (Stratagene). Two complementary oligonucleotides with mutated sequences for each mutant were used as primers (supplemental Table 1). The resulting kp60-NTD genes were sequenced to confirm the mutations. All proteins were purified with glutathione-Sepharose (GE Healthcare) and dialyzed against a buffer containing 50 mM Tris-HCl and 150 mM NaCl (pH 7.5). For pulldown assay, 80 pmol of GST (negative control) or GST fusion proteins were mixed with 10 μl of glutathione-Sepharose 4B (GE Healthcare) in 100 μl of binding buffer containing 80 mM PIPES-KOH (pH 6.8), 0.5 mM EGTA, and 2 mM $MgCl_2$ for 1 h at 4 °C. After washing the beads, 182 pmol (10 μg) of porcine tubulin (Cytoskeleton) was mixed in 200 μl of binding buffer for 2 h at 4 °C. The beads were washed three times, and the associated proteins were eluted with 50 mM Tris-HCl and 10 mM reduced glutathione (pH 7.5). The eluted proteins were resolved by SDS-PAGE and stained with silver.

Model Building—A molecular model of the complex of kp60-NTD with a tubulin tetramer was constructed manually using MOLMOL (33) on the basis of the complex between Vps4a-MIT and CHMP1a (PDB code 2jq9). First, the kp60-NTD structure determined in this study was superimposed onto the corresponding position of Vps4a-MIT. Then the tubulin tetramer, taken from PDB code 3du7, was superimposed onto the C-terminal helix of CHMP1a with the best one position selected out of the eight candidate positions of tubulin.

RESULTS

Structural Prediction and Sequence Analysis of kp60-NTD—Prior to structural determination, we extensively analyzed residues 1–90 of the N-terminal sequences of mouse and human kp60, which represent the sequences preceding the AAA domains, by both bioinformatics and biophysical methods (17). In brief, we found that these regions are genetically conserved only within a single subfamily of type I AAA-ATPase, corresponding to kp60 orthologs (Fig. 1*B*). Members of this family are found in mammals, other vertebrates, plants, insects, urchins, and nematodes, but not in yeasts or bacteria. It should be noted that some archaeal kp60s (*e.g.* gi: 13814089 and 223478990) that lack this N-terminal region are less well related

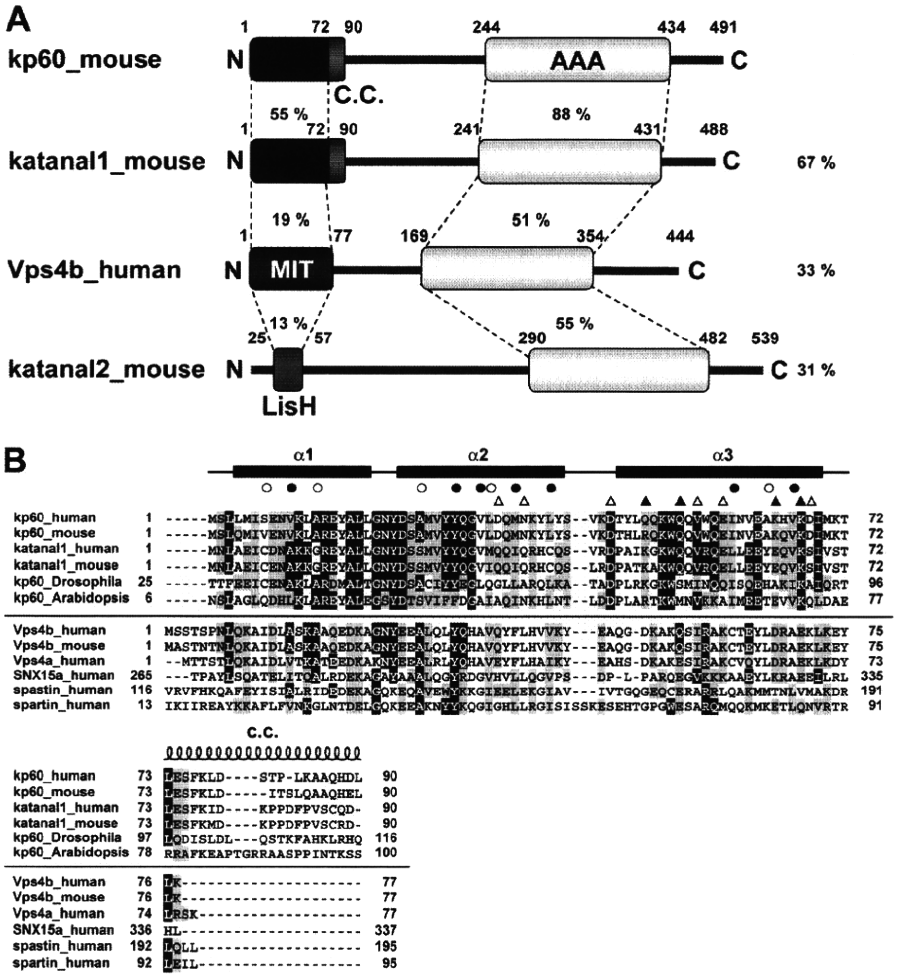

FIGURE 1. **Domain architectures and multiple sequence alignment of kp60s and proteins containing MIT domains.** *A*, domain architectures of mouse kp60, katanal1 and -2, and human Vps4b. The amino acid identities of each domain and full-length proteins between kp60 and other proteins are indicated. *C.C.*, coiled-coil; *MIT*, MIT domain; *LisH*, LIS1 homology domain; *AAA*, AAA domain. *B*, multiple sequence alignment of kp60-NTDs and related proteins with secondary structure elements of kp60-NTD. The secondary structure elements are shown at the *top* of the figure. The α-helices (α1–3) are represented as *thick lines* and the *C.C.* region as a coil. *Filled* and *open circles above* the alignments indicate well conserved and less conserved core residues, respectively (see Fig. 2*A*). *Triangles* indicate residues substituted with Ala for examining tubulin binding. (*Filled triangle*, involved in tubulin binding; *open triangle*, not involved.) Protein names and UniProtKB accession numbers are as follows: kp60 human (O75449); kp60 mouse (Q9WV86); kp60 *Drosophila* (Q9VN89); kp60 *Arabidopsis* (Q9SEX2); katanal1 human (Q9BW62); katanal1 mouse (Q8K0T4); Vps4b human (O75351); Vps4b mouse (P46467); Vps4a human (Q9UN37); SNX15a human (Q9NRS6); spartin human (Q8N0X7); and spastin human (Q9UBP0). The sequence alignment was generated by ClustalX (62).

to other kp60s, although a strong relationship is found for Vps4 orthologs. Thus, these archaeal kp60s may be better annotated as Vps4 homologs (35).

Focusing upon the AAA-ATPase domain and analyzing the domain level phylogenetic tree, the type I AAA-ATPases, including kp60, spastin, and Vps4, form a single cluster (7, 36). The kp60 orthologs with a conserved N-terminal region form a small subfamily, which is different from the Vps4 subfamily (supplemental Fig. 1). In some mammalian genomes (*e.g.* mouse, rat, and human), kp60-like A1s (katanal1s) are also conserved (Fig. 1). Katanal1s are very similar kp60 paralogs (~67% sequence identity over the entire chain). Moreover, this region (residues 1–90) can be further divided into two parts as follows: a well conserved core region (residues 1–72) and the following less-conserved region (~18 residues). The latter was a putative coiled-coil region, and the N-terminal region (residues 1–90) may form a dimer (17), whereas the first 72 residues behaved as an ideal "NMR ready" monomer. We call this region (residues 1–72) the core N-terminal domain (denoted kp60-NTD) and used it for further analysis.

Structure of kp60-NTD—kp60-NTD was analyzed by standard solution NMR techniques. All of the backbone and 96% of the nonexchangeable protons of the side chain signals were assigned. An ensemble of 20 structures with low CYANA target functions (Fig. 2*A*) was generated from 1723 experimental NMR constraints. These 20 structures satisfy the experimental constraints very well (Table 1). The stereochemical quality of the ensemble members is good, with all backbone ϕ/ψ angles occupying the most favored or additionally allowed regions of the Ramachandran plot (Table 1; supplemental Fig. 2). Excluding the disordered regions, *i.e.* the N-terminal region (residues 1–3 plus the preceding extra six residues of the tag) and the C-terminal region (residues 69–72), the r.m.s.d. values were 0.33 Å for backbone heavy atoms and 0.83 Å for all heavy atoms.

As shown in Fig. 2*B*, kp60-NTD is organized into antiparallel three-helix bundle that consists of helix 1 (4–19), helix 2 (23–41), and helix 3 (46–69). The secondary structure is shown in Fig. 1*B* along with its amino acid sequence. Helices 1 and 2 are connected by a very tight three-residue turn, whereas helices 2 and 3 are connected by a more flexible four-residue loop. Helices 2 and 3 are longer than helix 1, thereby exposing a large protrusion formed by helix 2 C terminus and helix 3 N terminus. These three helices are packed against one another nearly in parallel. The packing angles between the helices are similar as follows: 19.3° between 1 and 2, 21.1° between 2 and 3, and 26.1° between 1 and 3. Interhelical contacts mainly include hydrophobic side chain-side chain interactions. Core residues employed in these contacts are shown in Fig. 2*A* as well as in Fig. 1*B*. A total of 12 nonpolar contacts between helices 1 and 2, 17 between helices 2 and 3, and 5 between helices 1 and 3 were observed. The spatial arrangement of these three helices is nearly symmetric. The interhelical distances between helices 1

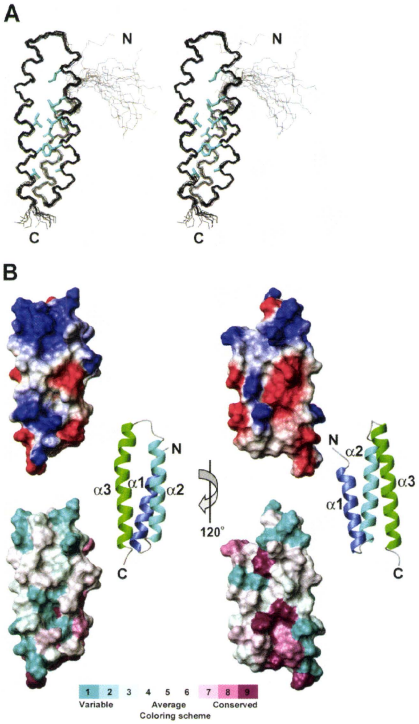

FIGURE 2. **Solution structure of kp60-NTD.** *A*, stereo view of the best fit superposition of the 20 structures with lowest target functions. Side chains of buried residues with solvent accessibility less than 10% are shown (*cyan*). *B*, *top*, electrostatic surface potential mapped onto a van der Waals surface diagram. The color scale ranges between $-20\ k_BT$ (*red*) to $+20\ k_BT$ (*blue*), where k_B is Boltzmann's constant and T is temperature. *Bottom*, sequence conservation among the kp60-NTDs is mapped on the surface. Conservative and variable residues are colored *purple* and *cyan*, respectively. The color codes were produced by ConSurf (63). Ribbon diagrams of the kp60-NTDs are shown in the *middle*. The surface composed of helices 2 and 3 is shown as the front view (*left*) and the rear view (*right*).

and 2 (5.0 Å) and helices 2 and 3 (5.5 Å) were shorter than that between helices 1 and 3 (6.5 Å). We found no obvious crevices or pockets on the surface of kp60-NTD. The kp60-NTD surface is highly charged (Fig. 2*B*).

Structural Similarities of kp60-NTD with MIT Domains and Other Tetratricopeptide Repeat Proteins—When the structure of kp60-NTD was subjected to DALI search (37), several MIT domains were first retrieved with Z-scores higher than 7.0, including NRBF-2 (PDB code 2crb, Z-score of 9.6, and r.m.s.d. of 1.6 Å), Vps4b (PDB code 1wr0, Z-score of 8.9, and r.m.s.d. of 2.7 Å), Vta1 (PDB code 2rkk, Z-score of 7.4, and r.m.s.d. of 2.4 Å), spastin (PDB code 3eab, Z-score of 7.2, and r.m.s.d. of 2.2 Å),

TABLE 1
Experimental restraints and statistics for 20 structures of kp60-NTD

Distance restraints	
Total no. of restraints	1723
Intraresidue	Unused
Sequential restraints ($\|i-j\|=1$)	831
Medium range restraints ($1<\|i-j\|\leq 4$)	462
Long range restraints ($\|i-j\|>4$)	304
Dihedral angle restraints	126
$\phi/\psi/\chi$	63/63/0
Hydrogen bond restraints	0
Statistics used for and obtained from the structure calculations	
Final Statistics (20/100)	
Cutoffs, distance (0.3 Å) and angle (3.0°)	
Maximum target function	0.06
Maximum violations	
Distance violation	0.21 Å
Angle violation	9.15°
Coordinate precision (residues 4–68)	
Backbone r.m.s.d.	0.33 Å
Heavy atom r.m.s.d.	0.83 Å
Ramachandran plot statistics (%) (all residues)	
Residues in most favored regions	92.2
Residues in additionally allowed regions	7.1
Residues in generously allowed regions	0.1
Residues in disallowed regions	0.0

and spartin (PDB code 2dl1, Z-score of 7.1, and r.m.s.d. of 2.4 Å). Thus, we first compared the structure of kp60-NTD with those of the MIT domains. Fig. 3 shows the structural comparisons between kp60-NTD and each of the MIT domains along with their sequence identity and structural fitness. Despite a low sequence similarity (10–19%), the kp60-NTD fold resembles those of the MIT domains, as shown by backbone r.m.s.d. of 2.2–2.7 Å for more than 67 residues from the secondary structural regions. Among these, spastin is the product of SPG4, which is mutated in the most common form of hereditary spastic paraplegia (4), and is involved with MT maintenance in axons (38, 39). Thus, the MIT domain of spastin is one of the closest homolog of kp60-NTD with regard to its physiological relevance to MT severing.

After comparing the structures in detail, all the helices were well superimposed, although the loop between helices 2 and 3 was not (Fig. 3*E*). The structures of the kp60 tubulin-binding site, kp60-NTD, and the MIT domain were strikingly similar, although their sequence similarity was very low (~19%). Thus, kp60-NTD is classified as a variant MIT domain. Because some of the MIT domains (*e.g.* spastin and spartin) are considered to bind microtubule (and/or tubulin), this structural similarity is not surprising.

One of the most characteristic features of the MIT domain is its unique hydrophobic core formed by conserved Ala residues, referred to as the "Ala zipper" (40, 41). These are thus identified as the key residues for the MIT domain signature (Ala-Xaa$_6$-Ala-Xaa$_{11}$-Ala-Xaa$_6$-Ala). These conserved Ala residues are present along the buried surfaces of helices 1–3 facing each other, thereby forming a hydrophobic core. In kp60 and its closely related homologs, these key Ala residues are only partly conserved. For example, Ile-6 and Val-32 in mouse kp60-NTD correspond to the zipper-forming Ala residues (Ala-9 and Ala-35) in the human Vps4a-MIT domain. Although the MIT domain signature is not conserved in kp60-NTD, this domain is obviously a close variant of the MIT domain. This imperfect conservation of the MIT-domain signature may explain why methods such as PSI-BLAST (18) and HMMER (19) could not

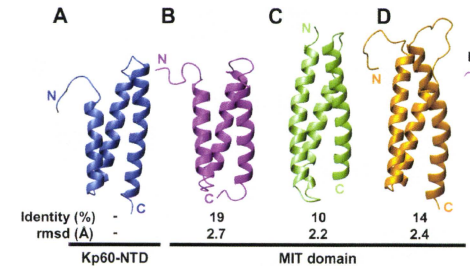

FIGURE 3. **Structural comparisons of kp60-NTD with MIT domains.** Ribbon diagrams of the proteins are as follows: *A*, kp60 (PDB code 2rpa); *B*, Vps4b (PDB code 1wr0); *C*, spastin (PDB code 3eab); *D*, spartin (PDB code 2dl1). Identity (*top*, %) and r.m.s.d. (*bottom*, Å) between kp60-NTD and the MIT domains are also presented. *E*, superposition of kp60-NTD (*blue*), Vps4b-MIT (*magenta*), spastin-MIT (*pale green*), and spartin-MIT (*orange*).

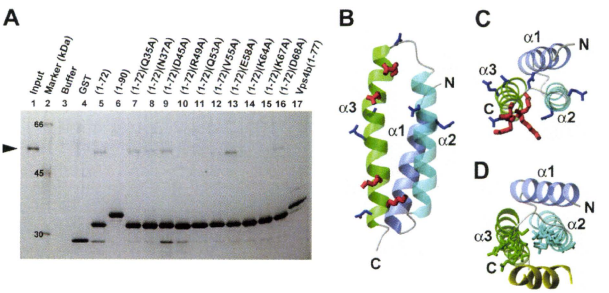

FIGURE 4. **Interactions of kp60-NTD with tubulin.** *A*, pulldown assays of tubulin with GST-tagged kp60-NTDs of wild type and Ala mutants and Vps4b-MIT *in vitro*. Tubulin was used as the input. Molecular size is shown in *lane 2*. Only the buffer and the GST tag used as negative controls are shown in *lanes 3* and *4*. Recombinant proteins used for pulldown are indicated at the top of the gel. SDS-PAGE was silver-stained. *B* and *C*, side and top views of the ribbon diagram of kp60-NTD, respectively. Side chains of residues that were substituted with Ala are shown. In the pulldown assay, residues that were affected and unaffected by Ala mutations for tubulin binding are colored *red* and *blue*, respectively. *D*, top view of the ribbon diagram of the complex between Vps4-MIT and CHMP1a (*yellow*) (PDB code 2jq9). Side chains of the residues interacting between Vps4 and CHMP1a are indicated.

predict the structural similarity between kp60-NTD and the MIT domain. In the DALI search, we also found other proteins containing either twisted α-helical hairpins or tetratricopeptide repeat motifs with Z-scores higher than 5.0. For example, partial structures of glycine-tRNA synthetase α-chain (PDB code 1j5w, Z-score of 8.7, and r.m.s.d. of 2.2 Å), 14-3-3 protein Tau (PDB code 2btp, Z-score of 8.2, and r.m.s.d. of 2.4 Å), cyclophilin 40 (PDB code 1ihg, Z-score of 8.1, and r.m.s.d. of 2.7 Å), α-E-catenin (PDB code 1l7c, Z-score of 7.9, and r.m.s.d. of 2.0 Å), fkbp52 (PDB code 1p5q, Z-score of 7.5, and r.m.s.d. of 3.0 Å), invertase inhibitor Nt-CIF (PDB code 1rj1, Z-score of 6.3, and r.m.s.d. of 2.1 Å), and Hop (PDB code 1elr, Z-score of 5.2, and r.m.s.d. of 3.7 Å) were shown to resemble kp60-NTD (data not shown).

Tubulin Binding by kp60-NTDs—To examine the molecular function of kp60-NTD as an MT binding domain, we performed *in vitro* MT binding assays using polymerized MTs. Contrary to our expectation, we found that the amount of kp60-NTD co-sedimented with MTs was very low, at the limit of detectability (supplemental Fig. 3) (data not shown). However, kp60-NTD co-sedimented with medium size MTs (supplemental Fig. 3*D*). These results suggested that kp60-NTD might bind to oligomeric tubulin and/or MT fragments rather than enormous polymerized MTs. Thus, we did a pulldown assay using GST-tagged kp60-NTD with unpolymerized tubulin. *In vitro* tubulin binding activity of kp60-NTD was observed (Fig. 4*A*, *lane 5*).

This tubulin binding activity varied with the length of the N-terminal domain. kp60-NTD (residues 1–72) binds tubulin, whereas kp60-NTD (residues 1–90) does not (Fig. 4*A*, *lane 6*). In our previous report, we showed that kp60-NTD (residues 1–90) formed a dimer using the coiled-coil region (residues 73–90) (17). Thus, dimer formation may hide the interface of kp60-NTD from tubulin. In addition, we found that the Vps4b-MIT domain (residues 1–77) did not bind tubulin (Fig. 4*A*, *lane 17*). Thus, the observed tubulin binding activity is specific for kp60-NTD.

Tubulin-binding Site of kp60-NTD—To determine the interfacial residues on kp60-NTD involved with tubulin recognition, we carried out mutagenesis experiments. Prior to these experiments, we attempted to identify the tubulin-interacting residues on kp60-NTD by NMR titration experiments and failed. We observed unexpected severe signal broadening even at very low tubulin concentration, which made further NMR analysis difficult (data not shown). Then, 10 residues from kp60-NTD (Gln-35, Asn-37, Asp-45, Arg-49, Gln-53, Val-55, Glu-58, Lys-64, Lys-67, and Asp-68) were selected, and each was substituted with Ala. These residues were carefully selected from the surface residues located on helices 2 and 3. The binding activities of mutants were examined by pulldown experiments (Fig. 4*A*, *lanes 7–16*).

The most significant effects were observed in mutations of residues on helix 3 as follows: Arg-49, Gln-53, Lys-64, and Lys-67. All of these side chains are hydrophilic and are exposed to the surface composed of helices 2 and 3 (Fig. 4, *B* and *C*). In addition, three of the four key residues are positively charged, suggesting an electrostatic interaction between kp60-NTD and tubulin. These residues were not conserved in the Vps4b-MIT domain as well as in the other MIT domains, such as spastin and spartin (Fig. 1*B*). This result is partially consistent with the

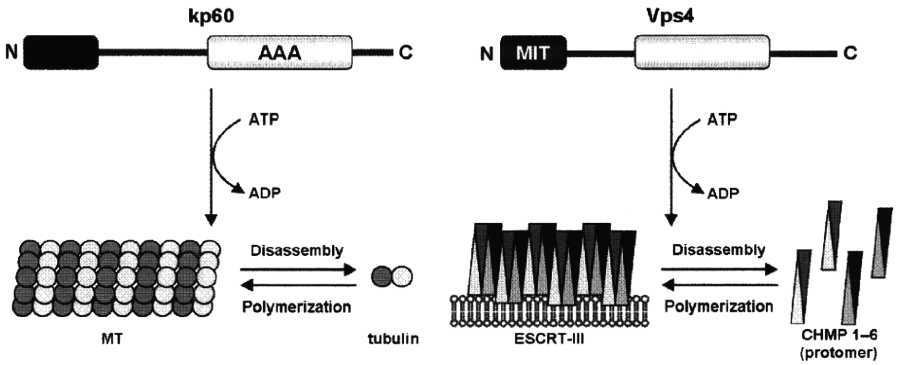

FIGURE 5. **Schematic diagram of architecture and molecular function similarities between kp60 and Vps4.** kp60 catalyzes the disassembly of MT via N-terminal domain binding, which results in MT severing. Vps4 catalyzes the release of the ESCRT-III protomer via the MIT domain binding, which results in endosomal membrane invagination. For both biological events, the N-terminal domains serve as adaptors for the polymeric macromolecules, thereby disassembling either the cytoskeleton or the membrane skeleton in an ATP-dependent manner.

inability of Vps4b-MIT to bind tubulin (Fig. 4*A*, *lane 17*). Because spastin and spartin can bind or regulate MTs (42, 43), this might indicate that these proteins bind MTs using regions other than the MIT domains. In contrast, mutants V55A, E58A, and D68A retained substantial tubulin binding activities (Fig. 4*A*, *lanes 12, 13,* and *16*). These residues are also on helix 3, but are exposed to the surface composed of helices 1 and 3 or outside of helix 3 (Fig. 4, *B* and *C*). Similarly, residues in helix 2 (Gln-35 and Asn-37) and loop 2 (Asp-45) were not involved in tubulin binding (Fig. 4*A*, *lanes 7–9*).

We further examined whether full-length kp60s with or without mutation in the N-terminal domain bind tubulin. We generated GST-tagged full-length kp60 in *E. coli*. Prior to the binding assay, we confirmed that the recombinant full-length kp60s had ATPase activity, according to the protocol in the recent paper (supplemental Fig. 4*A*) (16). We then performed pulldown experiments using mutants R49A and K67A of full-length kp60. The full-length kp60 (wild type) bound tubulin, whereas the mutants lacked tubulin binding activities, as expected by the results of kp60-NTDs (supplemental Fig. 4*B*; Fig. 4*A*).

DISCUSSION

Structural and Functional Comparisons with Other Tubulin Binding Domains—In this study, we have determined the structure of a novel tubulin binding domain derived from the conserved region of kp60, which was classified as a variant MIT domain. To our knowledge, this is the first experimental evidence for the direct interaction between an isolated MIT domain and tubulin.

To date, structures of many MT and/or tubulin binding domains have been determined (supplemental Fig. 5) (44–49). Interestingly, all-α-helical protein domains are dominant in these with solved structures, which might be advantageous for interactions with MT and/or tubulin. In the MT structure, the only accessible surface of tubulin includes helices 11 and 12 and the C-terminal tail (49–51). Thus, for one of tubulin recognition, helix-helix interactions of tubulin binding domains are suggested, although there are many structures of the known MT-interacting proteins left unsolved.

Structural and Functional Similarities to Vps4—We identified the tubulin-binding interface of kp60-NTD, which is on the surface comprising helices 2 and 3 (Fig. 4*B*). This result is consistent with the studies by Stoppin-Mellet, in which a truncation mutant of *Arabidopsis* kp60 (*At*KSS) that lacked the N-terminal 15 residues corresponding to helix 1 still retained MT severing activity (16). Surprisingly, the tubulin binding interface is very similar to the substrate (Vps2 and CHMP1a)-binding interfaces of the MIT domains of Vps4 (Fig. 4, *C* and *D*) (35, 52, 53). In other words, the common substrate-binding interfaces appear to be preserved between MT severing and membrane skeletal reorganization.

In studies of Vps4-MIT complexed with C-terminal regions of Vps2 or CHMP1a, the MIT domains use helices 2 and 3 as the interface for the α-helical peptides (35, 52). The residues involved with kp60-NTD-tubulin interaction are relatively conserved among kp60 orthologs (Fig. 1*B*), but they are not conserved between kp60-NTD and the other MIT domains, thus explaining why Vps4-MIT did not bind tubulin (Fig. 4*A*, *lane 17*). In contrast, another interface of Vps4-MIT for CHMPs has been reported, in which Vps4-MIT uses a shallow cleft between helices 1 and 3 for binding a proline-rich, CHMP6-derived peptide named MIT-interacting motif 2 (MIM2) (53). In the structure of kp60-NTD, there was no correspondence between helices 1 and 3, as the interhelical distance was substantially narrower (6.5 Å) than that of Vps4-MIT. We do not rule out the possibility that the interface composed of helices 1–3 serves as the binding site of other factors, such as katanin p80 and NDEL1 (54), both of which regulate the subcellular localization of kp60.

Conserved Macromolecular Disassembling Mechanisms between Vps4 and Kp60—Our findings indicate that the molecular architectures of kp60 and Vps4 are very similar in the following points: domain organization, structures of the N-terminal domains, and the relative locations of the interfaces for target proteins. Here, we propose some common features of the molecular mechanisms in different biological processes, MT severing and late endosomal luminal membrane budding, driven by kp60 and Vps4, respectively.

First, both the enzymes disassemble polymeric macromolecular complexes known as cytoskeleton and membrane skeleton. Second, these enzymes release protomers from macromolecular complexes (MT and ESCRT-III) in the cytoplasm depending on ATP hydrolysis. Finally, their N-terminal domains serve as adaptors to the protomers. The similarities of these mechanisms are illustrated in Fig. 5.

The ESCRT-III complex is composed of self-associating coiled-coil proteins (CHMP1–6), which form filamentous circular structures on the membrane surface (55). When Vps4 interacts with ESCRT-III filaments, it pulls out CHMP pro-

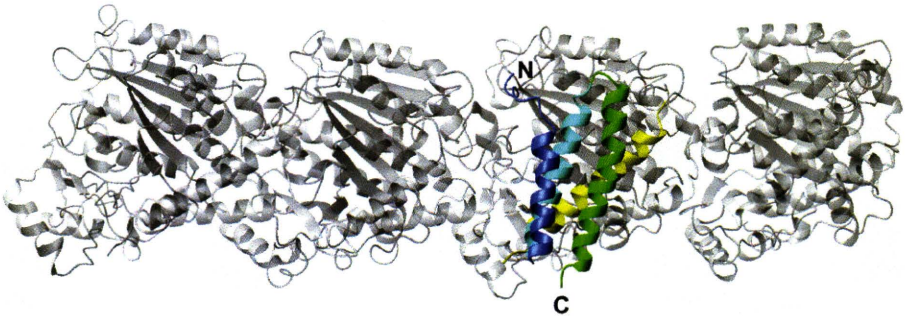

FIGURE 6. **Model of α-tubulin binding with kp60-NTD.** Ribbon diagram of a model complex between kp60-NTD and a tubulin tetramer (*gray*) is shown. α-Tubulin helix 12, a putative interface of kp60-NTD, is colored *yellow*.

tomers from the filamentous circular structure. The residual filaments of ESCRT-III then reorganize into a smaller circular structure by self-association. Vps4 continues to pull protomers away, and the circular structure shrinks into a smaller wheel. Finally, this downsizing of the ESCRT-III circle results in membrane budding with concomitant alterations of the membrane structure. This model is known as the "concentric circle model" (56).

We propose that the early stage of MT severing might have a similar mechanism. kp60 pulls a tubulin α/β-dimer away from MT in an ATP-dependent manner. However, contrary to the ESCRT-III polymer, polymerization of tubulin dimers is restricted to the plus end of MT as well as to the GTP form of tubulin, whereas polymerization at the minus end is extremely slow (reviewed in Refs. 1, 57). It is expected that once tubulin is pulled away by kp60, it can no longer fill the gap on MT. If two or more tubulin dimers are pulled away from this gap, then MT may start severing, resulting in a catastrophe. The structural similarities between kp60 and Vps4 revealed in this study encourage us to propose a model for the molecular mechanism of MT severing.

Model for kp60-NTD Binding to Tubulin Oligomer—To assess the detailed mechanism of MT severing, we constructed a model for the complex between kp60-NTD and a tubulin tetramer (Fig. 6). Our study is confined to the interface of the kp60 N-terminal adaptor domain to its tubulin substrate, as we did not identify the kp60-binding site on tubulin. Nevertheless, numerous literature resources provide a basis for model construction as follows. As discussed previously, the major candidates of the structural elements of tubulin that are accessible from outside MT are helices 11 and 12 (49–51). Next, the similarity between the interfaces of kp60-NTD with tubulin and that of Vps4-MIT with CHMP1a suggests that a helix on tubulin, which is similar to the CHMP1a helix (residues 115–127) bound to Vps4-MIT (52), may serve as the binding site of kp60. Taking all the information into account, we propose a model for the tubulin + kp60-NTD complex (Fig. 6).

While constructing the model, the following points were hypothesized: (i) one of the last helices (helix 11 or 12) makes contact with kp60-NTD at its helix 2/3 interface; (ii) the relative position and orientation between kp60-NTD and one of the tubulin helices mimic those between Vps4-MIT and the CHMP1a helix; (iii) steric crash between kp60-NTD and tubulin should be avoided; and (iv) charge-charge interactions between kp60-NTD and the tubulin helix should be maximized.

As a result, we found the following four candidate positions on tubulin C-terminal helices for kp60-NTD binding: (i) helix 11 (residues 386–396); (ii) helix 11 (residues 390–400); (iii) helix 12 (residues 420–430); and (iv) helix 12 (residues 423–433). All these positions are present on both tubulin-α and tubulin-β. Finally, by assessing complementarity of charge interactions in the model, the final model was selected out of the eight candidate models. Its helix 12 (residues 420–430) of tubulin α3 binds with kp60-NTD by occupying the corresponding position of CHMP1a (residues 115–127) that binds Vps4-MIT (PDB code 2jq9) (Fig. 6; supplemental Fig. 6) (52).

Alternatively, we generated the model of kp60-NTD + tubulin tetramer complex based on the complex between spastin-MIT with CHMP1b (PDB code 3eab) in which spastin-MIT used helices 1 and 3 as the interface to CHMP1b (supplemental Fig. 7) (58). This model is not consistent with our mutation studies (Fig. 4). Consequently, we justified the modeling of helices 2 and 3 as the tubulin-binding site. Because CHMP1b serves as an adaptor of spastin but not a substrate, this alternative model suggests that the helix 1/3 surface of kp60-NTD is a putative binding site for kp80, an adaptor of kp60 to bound MT and/or tubulin.

In the model of Fig. 6, the direction of the pore of the hexameric AAA-ATPase domain, which follows C-terminal to kp60-NTD, may approach the C-terminal tail of tubulin. We further confirmed this idea by using the model structure of full-length hexameric kp60 complexes with tubulin (supplemental Fig. 8). The location is consistent with the hypothesis that the pore of the AAA domain "sucks in" the tubulin C-terminal tail upon ATP hydrolysis (threading model) (59, 60). In fact, the literature suggests that kp60 function requires its direct interaction with the C-terminal tail of tubulin. This is based on the observation that MT severing activity was abolished when MTs were pretreated with subtilisin (8). Additional evidence regarding the MT-severing mechanism of spastin, another related AAA-ATPase, may support this idea. Spastin also recognizes and pulls the tubulin C-terminal tail as an initial binding site that is indispensable for its MT severing activity (42, 61). The hypotheses derived from our complex model require confirmation by additional experimentation.

In conclusion, the structure and key residues of kp60-NTD provide new insights into the molecular mechanisms of how the enzyme severs MT. The similarities of the molecular mechanisms as well as of the domain organizations suggest that these are evolutionally conserved among type I AAA-ATPases, kp60 and Vps4, whose cellular functions are distinct.

Acknowledgment—We thank Kaori Satomura for technical assistance.

REFERENCES

1. Desai, A., and Mitchison, T. J. (1997) *Annu. Rev. Cell Dev. Biol.* **13,** 83–117
2. Wittmann, T., Hyman, A., and Desai, A. (2001) *Nat. Cell Biol.* **3,** E28–E34
3. Zhang, D., Rogers, G. C., Buster, D. W., and Sharp, D. J. (2007) *J. Cell Biol.* **177,** 231–242
4. Hazan, J., Fonknechten, N., Mavel, D., Paternotte, C., Samson, D., Artiguenave, F., Davoine, C. S., Cruaud, C., Dürr, A., Wincker, P., Brottier, P., Cattolico, L., Barbe, V., Burgunder, J. M., Prud'homme, J. F., Brice, A., Fontaine, B., Heilig, B., and Weissenbach, J. (1999) *Nat. Genet.* **23,** 296–303
5. Errico, A., Ballabio, A., and Rugarli, E. I. (2002) *Hum. Mol. Genet.* **11,** 153–163
6. Cox, G. A., Mahaffey, C. L., Nystuen, A., Letts, V. A., and Frankel, W. N. (2000) *Nat. Genet.* **26,** 198–202
7. Frickey, T., and Lupas, A. N. (2004) *J. Struct. Biol.* **146,** 2–10
8. McNally, F. J., and Vale, R. D. (1993) *Cell* **75,** 419–429
9. Hartman, J. J., Mahr, J., McNally, K., Okawa, K., Iwamatsu, A., Thomas, S., Cheesman, S., Heuser, J., Vale, R. D., and McNally, F. J. (1998) *Cell* **93,** 277–287
10. McNally, K. P., Bazirgan, O. A., and McNally, F. J. (2000) *J. Cell Sci.* **113,** 1623–1633
11. McNally, F. J., Okawa, K., Iwamatsu, A., and Vale, R. D. (1996) *J. Cell Sci.* **109,** 561–567
12. McNally, F. J., and Thomas, S. (1998) *Mol. Biol. Cell* **9,** 1847–1861
13. Hartman, J. J., and Vale, R. D. (1999) *Science* **286,** 782–785
14. Lupas, A. N., and Martin, J. (2002) *Curr. Opin. Struct. Biol.* **12,** 746–753
15. Ogura, T., and Wilkinson, A. J. (2001) *Genes Cells* **6,** 575–597
16. Stoppin-Mellet, V., Gaillard, J., Timmers, T., Neumann, E., Conway, J., and Vantard, M. (2007) *Plant Physiol. Biochem.* **45,** 867–877
17. Iwaya, N., Goda, N., Unzai, S., Fujiwara, K., Tanaka, T., Tomii, K., Tochio, H., Shirakawa, M., and Hiroaki, H. (2007) *J. Biomol. NMR* **37,** 53–63
18. Altschul, S. F., Madden, T. L., Schäffer, A. A., Zhang, J., Zhang, Z., Miller, W., and Lipman, D. J. (1997) *Nucleic Acids Res.* **25,** 3389–3402
19. Bateman, A., Birney, E., Cerruti, L., Durbin, R., Etwiller, L., Eddy, S. R., Griffiths-Jones, S., Howe, K. L., Marshall, M., and Sonnhammer, E. L. (2002) *Nucleic Acids Res.* **30,** 276–280
20. Bateman, A., Coin, L., Durbin, R., Finn, R. D., Hollich, V., Griffiths-Jones, S., Khanna, A., Marshall, M., Moxon, S., Sonnhammer, E. L., Studholme, D. J., Yeats, C., and Eddy, S. R. (2004) *Nucleic Acids Res.* **32,** D138–D141
21. Letunic, I., Copley, R. R., Schmidt, S., Ciccarelli, F. D., Doerks, T., Schultz, J., Ponting, C. P., and Bork, P. (2004) *Nucleic Acids Res.* **32,** D142–D144
22. Tomii, K., and Akiyama, Y. (2004) *Bioinformatics* **20,** 594–595
23. Shi, J., Blundell, T. L., and Mizuguchi, K. (2001) *J. Mol. Biol.* **310,** 243–257
24. Ciccarelli, F. D., Proukakis, C., Patel, H., Cross, H., Azam, S., Patton, M. A., Bork, P., and Crosby, A. H. (2003) *Genomics* **81,** 437–441
25. Goda, N., Tenno, T., Takasu, H., Hiroaki, H., and Shirakawa, M. (2004) *Protein Sci.* **13,** 652–658
26. Yamazaki, T., Lee, W., Arrowsmith, C. H., Muhandiram, D. R., and Kay, L. E. (1994) *J. Am. Chem. Soc.* **116,** 11655–11666
27. Cavanagh, J., Fairbrother, W. J., Palmer, A. G., 3rd, Rance, M., and Skelton, N. J. (2007) *Protein NMR Spectroscopy: Principles and Practice*, 2nd Ed., pp. 535–673, Academic Press, San Diego
28. Delaglio, F., Grzesiek, S., Vuister, G. W., Zhu, G., Pfeifer, J., and Bax, A. (1995) *J. Biomol. NMR* **6,** 277–293
29. Goddard, T. D., and Kneller, D. G. (2004) *SPARKY*, Version 3, University of California, San Francisco
30. Herrmann, T., Güntert, P., and Wüthrich, K. (2002) *J. Mol. Biol.* **319,** 209–227
31. Guntert, P. (2003) *Prog. Nucleic Magn. Reson. Spect.* **43,** 105–125
32. Cornilescu, G., Delaglio, F., and Bax, A. (1999) *J. Biomol. NMR* **13,** 289–302
33. Koradi, R., Billeter, M., and Wuthrich, K. (1996) *J. Mol. Graph.* **14,** 29–32
34. Laskowski, R. A., Rullmannn, J. A., MacArthur, M. W., Kaptein, R., and Thornton, J. M. (1996) *J. Biomol. NMR* **8,** 477–486
35. Obita, T., Saksena, S., Ghazi-Tabatabai, S., Gill, D. J., Perisic, O., Emr, S. D., and Williams, R. L. (2007) *Nature* **449,** 735–739
36. Fröhlich, K. U. (2001) *J. Cell Sci.* **114,** 1601–1602
37. Holm, L., and Sander, C. (1997) *Nucleic Acids Res.* **25,** 231–234
38. Sherwood, N. T., Sun, Q., Xue, M., Zhang, B., and Zinn, K. (2004) *PLoS. Biol.* **2,** e429
39. Evans, K. J., Gomes, E. R., Reisenweber, S. M., Gundersen, G. G., and Lauring, B. P. (2005) *J. Cell Biol.* **168,** 599–606
40. Takasu, H., Jee, J. G., Ohno, A., Goda, N., Fujiwara, K., Tochio, H., Shirakawa, M., and Hiroaki, H. (2005) *Biochem. Biophys. Res. Commun.* **334,** 460–465
41. Scott, A., Gaspar, J., Stuchell-Brereton, M. D., Alam, S. L., Skalicky, J. J., and Sundquist, W. I. (2005) *Proc. Natl. Acad. Sci. U.S.A.* **102,** 13813–13818
42. White, S. R., Evans, K. J., Lary, J., Cole, J. L., and Lauring, B. (2007) *J. Cell Biol.* **176,** 995–1005
43. Patel, H., Cross, H., Proukakis, C., Hershberger, R., Bork, P., Ciccarelli, F. D., Patton, M. A., McKusick, V. A., and Crosby, A. H. (2002) *Nat. Genet.* **31,** 347–348
44. Ravelli, R. B., Gigant, B., Curmi, P. A., Jourdain, I., Lachkar, S., Sobel, A., and Knossow, M. (2004) *Nature* **428,** 198–202
45. Slep, K. C., and Vale, R. D. (2007) *Mol. Cell* **27,** 976–991
46. Mishima, M., Maesaki, R., Kasa, M., Watanabe, T., Fukata, M., Kaibuchi, K., and Hakoshima, T. (2007) *Proc. Natl. Acad. Sci. U.S.A.* **104,** 10346–10351
47. Guasch, A., Aloria, K., Pérez, R., Avila, J., Zabala, J. C., and Coll, M. (2002) *J. Mol. Biol.* **318,** 1139–1149
48. Carter, A. P., Garbarino, J. E., Wilson-Kubalek, E. M., Shipley, W. E., Cho, C., Milligan, R. A., Vale, R. D., and Gibbons, I. R. (2008) *Science* **322,** 1691–1695
49. Kikkawa, M., and Hirokawa, N. (2006) *EMBO J.* **25,** 4187–4194
50. Nogales, E., Wolf, S. G., and Downing, K. H. (1998) *Nature* **391,** 199–203
51. Bodey, A. J., Kikkawa, M., and Moores, C. A. (2009) *J. Mol. Biol.* **388,** 218–224
52. Stuchell-Brereton, M. D., Skalicky, J. J., Kieffer, C., Karren, M. A., Ghaffarian, S., and Sundquist, W. I. (2007) *Nature* **449,** 740–744
53. Kieffer, C., Skalicky, J. J., Morita, E., De Domenico, I., Ward, D. M., Kaplan, J., and Sundquist, W. I. (2008) *Dev. Cell* **15,** 62–73
54. Toyo-Oka, K., Sasaki, S., Yano, Y., Mori, D., Kobayashi, T., Toyoshima, Y. Y., Tokuoka, S. M., Ishii, S., Shimizu, T., Muramatsu, M., Hiraiwa, N., Yoshiki, A., Wynshaw-Boris, A., and Hirotsune, S. (2005) *Hum. Mol. Genet.* **14,** 3113–3128
55. Hanson, P. I., Roth, R., Lin, Y., and Heuser, J. E. (2008) *J. Cell Biol.* **180,** 389–402
56. Nickerson, D. P., Russell, M. R., and Odorizzi, G. (2007) *EMBO Rep.* **8,** 644–650
57. Howard, J., and Hyman, A. A. (2003) *Nature* **422,** 753–758
58. Yang, D., Rismanchi, N., Renvoisé, B., Lippincott-Schwartz, J., Blackstone, C., and Hurley, J. H. (2008) *Nat. Struct. Mol. Biol.* **15,** 1278–1286
59. Sauer, R. T., Bolon, D. N., Burton, B. M., Burton, R. E., Flynn, J. M., Grant, R. A., Hersch, G. L., Joshi, S. A., Kenniston, J. A., Levchenko, I., Neher, S. B., Oakes, E. S., Siddiqui, S. M., Wah, D. A., and Baker, T. A. (2004) *Cell* **119,** 9–18
60. Lum, R., Tkach, J. M., Vierling, E., and Glover, J. R. (2004) *J. Biol. Chem.* **279,** 29139–29146
61. Roll-Mecak, A., and Vale, R. D. (2008) *Nature* **451,** 363–367
62. Thompson, J. D., Gibson, T. J., Plewniak, F., Jeanmougin, F., and Higgins, D. G. (1997) *Nucleic Acids Res.* **25,** 4876–4882
63. Armon, A., Graur, D., and Ben-Tal, N. (2001) *J. Mol. Biol.* **307,** 447–463

Supplementary materials for

A COMMON SUBSTRATE RECOGNITION MODE CONSERVED BETWEEN KATANIN P60 AND VPS4 GOVERNS MICROTUBULE SEVERING AND MEMBRANE SKELETON REORGANIZATION *

Naoko Iwaya[1,2,3], Yohta Kuwahara[2,3,4], Yoshie Fujiwara[2,5], Natsuko Goda[2,4], Takeshi Tenno[2,4], Kohei Akiyama[3], Shogo Mase[2,4], Hidehito Tochio[1], Takahisa Ikegami[6], Masahiro Shirakawa[1], Hidekazu Hiroaki[2,3,4,5]

[1]Department of Molecular Engineering, Graduate School of Engineering, Kyoto University
[2]Division of Structural Biology, Graduate School of Medicine, Kobe University, 7-5-1 Kusunokicho, Chuo, Kobe, Hyogo 650-0017, Japan
[3]Field of Supramolecular Biology, International Graduate School of Arts and Sciences, Yokohama City University
[4]Institute for Bioinformatics Research and Development (BIRD), Japan Science and Technology Corporation (JST)
[5]Global-COE (Center of Excellence) Program for Integrative Membrane Biology, Kobe University
[6]Institute of Protein Research, Osaka University

Running title: Structure of the N-terminal domain of katanin p60

Adress correspondence to : Hidekazu Hiroaki, PhD., e-mail: hiroakih@med.kobe-u.ac.jp, Phone: +81 78 382 5813 / Fax: +81 78 382 5816

SUPPLEMENTARY EXPERIMENTAL PROCEDURES

Production of Full-length kp60 - Expression vector for the recombinant GST-tagged full-length kp60 of mouse was constructed by standard protocol using PCR, and ligated into *BamHI-SalI* sites of pGEX-6P3 (GE Healthcare Bioscience). Ala-substituted mutants were engineered with QuikChange site-directed mutagenesis kit (Stratagene). The fusion proteins were produced in *E. coli* JM109. Expression was induced with 0.1 mM IPTG, and LB cultures were grown overnight at 20 °C. For pull-down assays, GST-tagged proteins were bound to glutathione-Sepharose 4B (GE Healthcare Bioscience) and washed with the storage buffer (20 mM Tris-HCl, pH 7.5, 150 mM NaCl, 1 mM $MgCl_2$, and 0.1 mM ATP) supplemented with EDTA-free protease inhibitor cocktail (Nacali tesque Inc, Kyoto, Japan) on column. GST-kp60s bound to glutathione-Sepharose were eluted with the elution buffer (50 mM Tris-HCl, 100 mM NaCl, 40 mM reduced glutathione, pH 8.0, and 5% glycerol). The eluents were further used for ATPase assays.

ATPase assays - ATPase activity was measured using an ATP regenerating system (1). The reaction mixture containing 50 mM Tris-HCl, pH 7.5, 50 mM KCl, 2 mM $MgCl_2$, 2 mM phosphoenolpyruvate, 1 mM ATP, 50 μg/ml pyruvate kinase, 50 μg/ml lactate dehydrogenase, and 0.2 mM NADH was used. The reactions were initiated by the addition of GST-kp60s (0.5 μM), and the activities were measured by monitoring the decrease of NADH absorption at 340 nm at room temperature using UV-Vis spectrophotometer, UV mini-1240 (Shimadzu, Tokyo, Japan). The data were normalized for further analysis.

Tubulin Binding Assays - 5 μg of GST-proteins bound to glutathione-Sepharose 4B (20 μl) were incubated with 10 μg of tubulin in the binding buffer (80 mM PIPES, pH 7.0, 1 mM $MgCl_2$ and 1 mM EGTA) for 30 min at 4°C. The beads were washed four times in the wash buffer (4.3 mM Na_2HPO_4, 1.47 mM KH_2PO_4, 137 mM NaCl, 2.7 mM KCl, pH 7.3, and 5% glycerol). The associated proteins were eluted in the elution buffer (50 mM Tris-HCl, 100 mM NaCl, 50 mM reduced glutathione, pH 8.0, and 5% glycerol). The eluted proteins were analyzed by SDS-PAGE and Western blotting.

Western Blotting - Proteins were resolved in SDS-PAGE and blotted onto a PVDF membrane. We detected tubulin using 1/2000 diluted anti-α-tubulin antibody (Siguma-Aldrich) followed by HRP-conjugated anti-mouse IgG secondary antibody (Promega). The proteins were visualized using an ECL-Plus kit (GE Healthcare Bioscience) and detected using LAS-1000 detector (Fuji Film, Tokyo, Japan).

Model building – A molecular model of the complex of kp60-NTD with a tubulin tetramer was constructed based on the complex between spastin-MIT and CHMP1b (PDB: 3eab). The kp60-NTD structure and the tubulin tetramer (3du7) were superimposed onto the corresponding position of spastin-MIT and the C-terminal helix of CHMP1b (174-193), respectively. The best model fully overrided on helices with binding sites was selected considering steric crash and complementary charge interactions between structures. A hexameric ring model of AAA ATPase domains of kp60 was generated by superimposing the Cα atoms of kp60 onto those of the hexameric ring structure of p97 D1 (PDB: 1s3s) using MODELLER (version 9v6) (http://salilab.org/modeller/). Finally, the complex model structure of hexameric full-length kp60 with tubulin oligomer was constructed using MOLMOL (2) by joining the components manually.

SUPPLEMENTARY FIGURE LEGENDS

Supplementary Fig. 1.
Phylogenetic tree of the AAA protein superfamily. Red circle, kp60 subfamily; Blue circle, Vps4 subfamily. The tree data were calculated by ClustalX (3) and the tree was drawn with TreeView (http://taxonomy.zoology.gla.ac.uk/rod/treeview.html).

Supplementary Fig. 2.
Ramachandran plot for the phi-psi values of the final 20 structures of kp60-NTD. This figure was produced using PROCHECK-NMR (4).

Supplementary Fig. 3.
Interactions between kp60-NTD and MTs/tubulin dimer. *A*, schematic diagram of pull-down assay using Microtubule binding protein spin down assay kit, BK029 (Cytoskeleton) to assess interactions between GST-tagged kp60-NTD and MTs/tubulin *in vitro*. GST-tagged kp60-NTD was mixed with a reaction solution after (upper left) and before (upper right) tubulin polymerization reaction, then ultracentrifuged. Tubulin was separated by molecular weight; polymerized MTs were sedimented at the bottom of tubes, non-polymerized tubulin migrated to the top of the solution (lower panel). Reaction solutions were divided into four fractions (from top to bottom) and each fraction was analyzed by SDS-PAGE. GST-tagged kp60-NTD co-sedimented with non-polymerized tubulin. *B*, the reaction solution after polymerization of only tubulin was ultracentrifuged and analyzed as a control. Lanes 1–4 correspond to fractions from top to bottom, indicated in the lower panels of *A*. *C*, pull-down assay for kp60-NTD mixed after tubulin polymerization reaction. kp60-NTD may possibly bind with a tubulin dimer rather than MTs. *D*, pull-down assays of the GST-tagged kp60-NTD mixed before tubulin polymerization reaction. SDS-PAGEs are Coomassie-stained.

Supplementary Fig. 4.
ATPase activity of full-length kp60 and interactions of kp60 with tubulin. *A*, ATPase activities of kp60s (0.5 μM) at 340 nm. Filled diamond (continuous line): wild type, filled box (dotted line): R49A, filled triangle (broken line): K67A. *B*, pull-down assays of tubulin with wild type (WT) of GST-kp60 and Ala mutants *in vitro*. Molecular size is shown in the left. Tubulin was used as the input. Only the buffer and the GST-tag mixed with tubulin as negative controls are shown in lanes 2 and 3. Recombinant proteins used for pull-down are indicated at the top of the gel. Filled and open arrowheads show tubulin and full-length kp60s, respectively. SDS-PAGE was Coomassie-stained (upper panel). Western blotting analysis of tubulin bound to full-length kp60s was visualized by ECL (lower panel).

Supplementary Fig. 5.
Comparison of structures and tubulin binding interfaces with other tubulin binding domains. Tubulin binding interfaces are indicated by black and arrows. *A*, stathmin-like domain bound to the tubulin (white) (PDB: 1sa1); *B*, EB1 CH domain (2qjz); *C*, Msps TOG2 domain (2qk2); *D*, CAP-Gly domain bound to the tubulin peptide (white) (2e4h), and *E*, tubulin-specific chaperone cofactor A (1h7c).

Supplementary Fig. 6.
Model for α–tubulin helix 12 binding with kp60-NTD. An electrostatic surface potential diagram (top), a ribbon diagram (middle), and a sequence conservation diagram (bottom) for kp60-NTD were shown. α–Tubulin helix 12 is shown as a transparent cylinder (yellow).

Supplementary Fig. 7.

Comparison between model for tubulin binding interfaces of kp60-NTD. *A*, model of kp60-NTD bound to α–tubulin at the helix 1/3 interface (see text). Ribbon diagram of the model complex between kp60-NTD and a tubulin tetramer (grey) was constructed based on the complex between spastin-MIT and CHMP1b (PDB: 3eab). α–tubulin helix 12, a putative interface to kp60-NTD, is colored yellow. *B* and *C*, side (top) and top (bottom) views of the ribbon diagram of the complex between kp60-NTD and α–tubulin using the helix 1/3 and helix 2/3 interfaces, respectively. Side chains of key residues for binding tubulin are shown (red). *D*, top view of the ribbon diagram of the complex between spastin-MIT and CHMP1b (yellow) (3eab). Side chains of the residues interacting between spastin and CHMP1b are indicated.

Supplementary Fig. 8.
Proposed model for tubulin binding with full-length kp60. Model complex between tubulin origomer (grey) and hexameric full-length kp60, composed of kp60-NTD and AAA ATPase domain (violet) is shown. AAA ATPase domains form hexameric ring. Five of the six kp60-NTDs on the hexameric AAA ATPase domains were not drawn for clarity. One of the tubulin C-terminal tail is shown in yellow. The tail on the surface of MT may bind to the pore of the hexameric AAA ATPase domain of kp60.

Supplementary Table 1.

Oligonucleotides used as primers for Ala substitution.

Primer	Sequence
Q35A_F	CAGGGAGTTCTTGAC**GCC**ATGAACAAGTACCTGTACTCAGTC
Q35A_R	GACTGAGTACAGGTACTTGTTCAT**GGC**GTCAAGAACTCCCTG
N37A_F	CAGGGAGTTCTTGACCAAATG**GCC**AAGTACCTGTACTCAGTC
N37A_R	GACTGAGTACAGGTACTT**GGC**CATTTGGTCAAGAACTCCCTG
D45A_F	CTGTACTCAGTCAAA**GCC**ACACACCTCCGTCAGAAATGG
D45A_R	CCATTTCTGACGGAGGTGTGT**GGC**TTTGACTGAGTACAG
R49A_F	GTCAAAGATACACACCTC**GCC**CAGAAATGGCAACAG
R49A_R	CTGTTGCCATTTCTG**GGC**GAGGTGTGTATCTTTGAC
Q53A_F	CTCCGTCAGAAATGG**GCC**CAGGTTTGGCAGGAAATAAATGTG
Q53A_R	CACATTTATTTCCTGCCAAACCTG**GGC**CCATTTCTGACGGAG
V55A_F	CTCCGTCAGAAATGGCAACAG**GCC**TGGCAGGAAATAAATGTG
V55A_R	CACATTTATTTCCTGCCA**GGC**CTGTTGCCATTTCTGACGGAG
E58A_F	CAGAAATGGCAACAGGTTTGGCAG**GCC**ATAAATGTGGAAGCTAAG
E58A_R	CTTAGCTTCCACATTTAT**GGC**CTGCCAAACCTGTTGCCATTTCTG
K64A_F	GTTTGGCAGGAAATAAATGTGGAAGCT**GCC**CAAGTTAAGGATATCATG
K64A_R	CATGATATCCTTAACTTG**GGC**AGCTTCCACATTTATTTCCTGCCAAAC
K67A_F	GTGGAAGCTAAGCAAGTT**GCC**GATATCATGAAAACATAATAGAGC
K67A_R	GCTCTATTATGTTTTCATGATATC**GGC**AACTTGCTTAGCTTCCAC
D68A_F	GTGGAAGCTAAGCAAGTTAAG**GCC**ATCATGAAAACATAATAGAGC
D68A_R	GCTCTATTATGTTTTCATGAT**GGC**CTTAACTTGCTTAGCTTCCAC

SUPPLEMENTARY REFERENCES

1. Hackney, D. D., and Jiang, W. (2001) *Methods Mol Biol* **164**, 65-71
2. Koradi, R., Billeter, M., and Wuthrich, K. (1996) *J Mol Graph* **14**, 29-32
3. Thompson, J. D., Gibson, T. J., Plewniak, F., Jeanmougin, F., and Higgins, D. G. (1997) *Nucleic Acids Res* **25**, 4876-4882
4. Laskowski, R. A., Rullmannn, J. A., MacArthur, M. W., Kaptein, R., and Thornton, J. M. (1996) *J Biomol NMR* **8**, 477-486

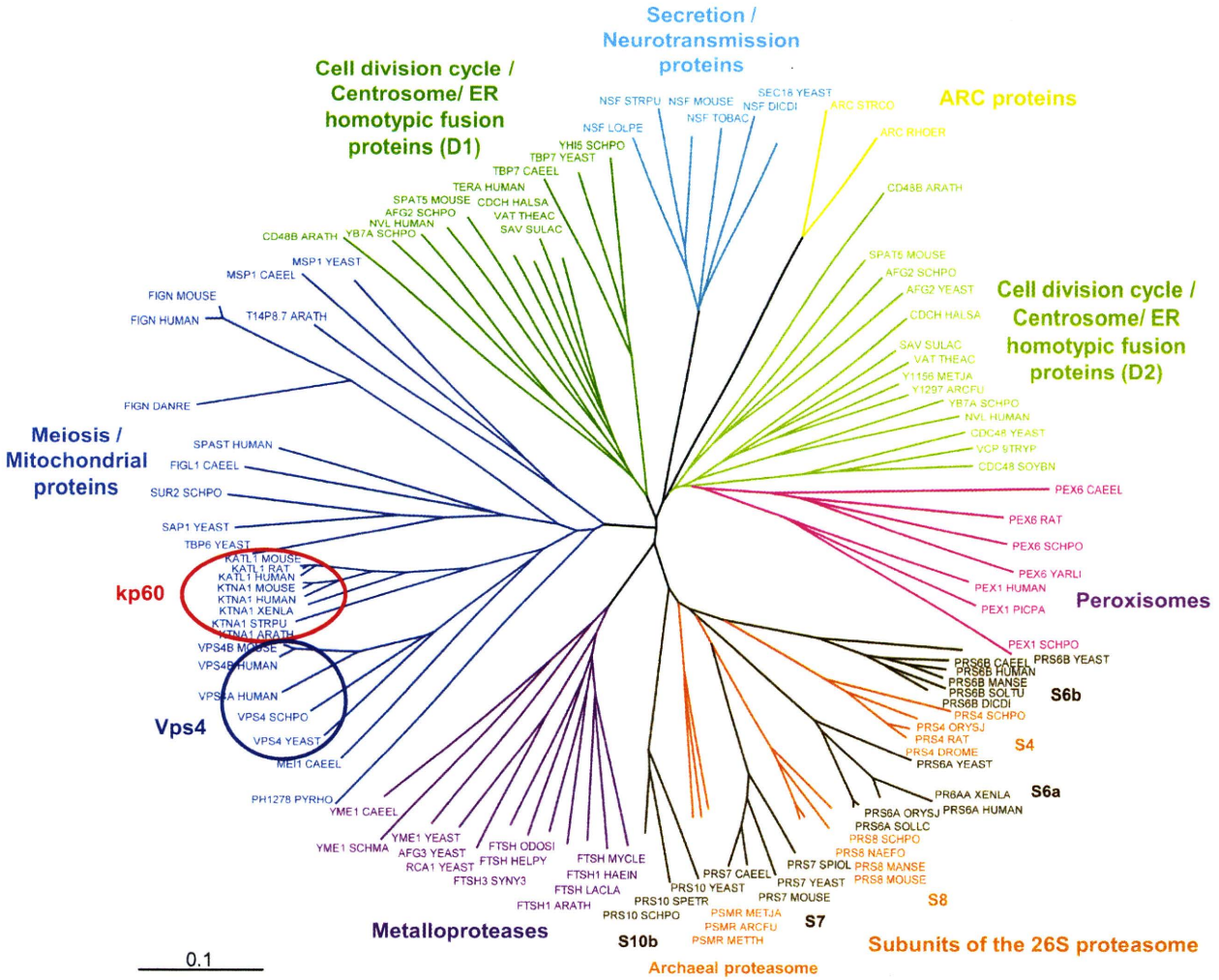

Supplementary Figure 1